ORIGINAL CONTRIBUTION

Numerical simulations of oscillatory shear flow of particle suspensions at finite inertia

Massimiliano M. Villone[1] (ORCID) · **Marco E. Rosti[2]** · **Outi Tammisola[2]** · **Luca Brandt[2]**

Abstract

We perform immersed-boundary-method numerical simulations of oscillatory shear flow of suspensions of mono-disperse non-colloidal rigid spherical particles in a Newtonian liquid from the dilute to the concentrated regime. Both small and large amplitude oscillatory shear flow (SAOS and LAOS, respectively) are studied and the effects of particle concentration, fluid inertia, particle-to-fluid density ratio, and deformation amplitude on the measured apparent viscoelastic moduli of the suspensions are quantified. In the SAOS regime, a non-zero storage modulus G' is always detected: inertia acts as an apparent elasticity. G'-values significantly change with inertia, but depend on the volume fraction of the solid phase only for suspensions of particles denser than the fluid. On the other hand, the loss modulus G'' increases with both inertia and particle concentration. In the LAOS regime, the moduli are only weakly dependent on the deformation amplitude for a dilute suspension, whereas non-monotonic variations are observed at high concentrations.

Keywords Rheology · Suspensions · Oscillatory shear flow · Inertia · Numerical simulations

Introduction

The term 'suspension' describes a multiphase fluid system where solid particles are suspended in a liquid, often called a 'solvent' or a 'matrix'. Suspensions have been extensively studied over the last century due to their relevant role in many technological processes, e.g. those occurring in oil, cement, paper, or food industries (see, for example, the review by Mewis and Wagner 2009, and the references therein). Therefore, the literature on suspension rheology is vast, with several theoretical, experimental, and numerical studies.

The most important parameters determining the flow behaviour of a suspension are the size, shape, and concentration of the solid fillers and the rheological behaviour of the suspending liquid. Particle concentration is usually measured in terms of the volume fraction of the suspended phase, ϕ, the suspension being identified as 'dilute' when $\phi \leq 0.05$, 'semi-dilute' for $0.05 \leq \phi \leq 0.1$, and 'concentrated' for $\phi > 0.1$. Of course, concentrated suspensions are the most likely to occur in actual applications (see, for example, the work by Barnes (2003), and the references therein). Concerning the suspending liquid, despite the fact that viscoelastic fluids are important in several technological fields (e.g. filled polymers, paints, coatings, foods), greater attention has been devoted in the literature to suspensions with Newtonian matrices.

The very first work dealing with the rheology of a suspension of non-colloidal spherical rigid particles in a Newtonian fluid dates back to the early twentieth century and is due to Einstein (1911), who theoretically derived that the shear viscosity of a dilute suspension linearly increases with ϕ according to the famous law

$$\eta_{\mathrm{s}} = \eta(1 + 2.5\phi), \tag{1}$$

with η_{s} the suspension viscosity and η the viscosity of the suspending liquid. Since then, numerous theoretical, experimental, and numerical papers have investigated the rheology of suspensions with Newtonian matrices. A very recent review of these studies is provided by Tanner (2018).

✉ Massimiliano M. Villone
massimiliano.villone@unina.it

[1] Dipartimento di Ingegneria Chimica, dei Materiali e della Produzione Industriale, Universitá degli Studi di Napoli Federico II, P.le Tecchio 80, 80125 Napoli, Italy

[2] Linné FLOW Centre and SeRC, KTH Mechanics, Osquars Backe 18, SE-100 44 Stockholm, Sweden

Relevant to the work presented here, we mention the numerical studies by Picano et al. (2013) and Alghalibi et al. (2018), who considered inertial effects in suspensions with Newtonian and inelastic non-Newtonian suspending media up to particle Reynolds numbers of order 10. These authors report shear-thickening, i.e. an increase of the suspension viscosity with the shear rate in the inertial regime (see also Kulkarni and Morris 2008). This is explained in terms of an increase of the suspension effective volume fraction related to the asymmetry of the particle-pair trajectories in the presence of inertia (the formation of a so-called shadow region). Although the dissipation in the flow is of viscous origin, inertia affects the suspension microstructure and thus increases the system effective viscosity.

Besides viscosity measurements in steady flows, oscillatory motions are often used in rheometry in order to determine the viscoelastic properties of complex fluids. If the rheometer performs small-amplitude oscillations and inertia is negligible, the stress in a non-colloidal suspension with a Newtonian matrix is in phase with the imposed oscillatory velocity. In other words, only a non-null loss modulus is detected, whereas no storage modulus is measured. In the linear regime, i.e. when the oscillations are 'small', the loss modulus G'' of the suspension reads

$$G'' = \eta\omega(1 + 2.5\phi), \tag{2}$$

where ω is the frequency of the oscillations.

Inertia is neglected in the definition of the fluid material properties related to oscillatory shear flows, namely, the storage modulus G' and the loss modulus G''. Nevertheless, it might come into play in many practical situations, especially when low-viscosity fluids and/or high oscillatory frequencies are considered. If the system is modelled as inertialess, this could lead to misinterpretation of the measurements and hence inaccurate predictions. For instance, Böhme and Stenger (1990) measured non-null values of the storage modulus G' in pure Newtonian liquids.

In this paper, we perform numerical simulations to investigate the effects of inertia on the (in silico) measurements of the viscoelastic moduli of suspensions of mono-disperse non-colloidal rigid spheres in a Newtonian fluid, from the dilute to the concentrated regime. First of all, we study the effects of inertia acting on suspension volume length scale on the values of the apparent storage and loss moduli of suspensions of neutrally buoyant spheres. Then, we also study the effects of micro-inertia, i.e. inertia acting on particle length scale, by considering suspensions of particles denser than the suspending fluid. We first study small amplitude oscillatory shear (SAOS) flow, and then introduce an additional source of non-linearity by extending the analysis to the large amplitude oscillatory shear (LAOS) flow regime.

Mathematical model

We consider the system schematically depicted in Fig. 1, i.e. initially randomly distributed mono-disperse non-colloidal rigid spheres with diameter D_p suspended in an incompressible Newtonian fluid undergoing oscillatory shear flow between two counter-sliding parallel plates, namely, in a plane Couette geometry. Here, x, y, and z (x_1, x_2, and x_3) denote the streamwise, wall-normal, and spanwise directions, whereas u_x, u_y, and u_z (u_1, u_2, and u_3) denote the corresponding components of the fluid velocity field. The lower and upper moving walls are located at $y = 0$ and $y = H$, and move streamwise in opposite directions with oscillating velocity $u_w(t) = (H/2)\gamma_0\omega\sin(\omega t)$, where γ_0 is the maximum deformation to which the system is subjected, ω is the oscillatory frequency, and t is time. A relevant geometrical parameter is the blockage ratio $\beta = D_p/H$, measuring the confinement of the particles. All the simulations reported in this paper are performed with $\beta = 0.2$, as in Picano et al. (2013), Alghalibi et al. (2018), Rosti and Brandt (2018) among others.

The motion of the fluid is governed by the continuity and the momentum balance equation in the incompressible formulation, i.e. the Navier-Stokes equations, that, when gravity is neglected, read

$$\nabla \cdot \mathbf{u} = 0, \tag{3}$$

$$\rho\left(\frac{\partial \mathbf{u}}{\partial t} + \mathbf{u} \cdot \nabla \mathbf{u}\right) = \nabla \cdot \boldsymbol{\sigma} + \mathbf{f}, \tag{4}$$

where ρ is the fluid density, $\mathbf{u}$ is its velocity, $\boldsymbol{\sigma}$ is the Cauchy stress tensor, and $\mathbf{f}$ is a body force used to account for the presence of the rigid particles. The fluid is assumed to be Newtonian with the constitutive equation

$$\boldsymbol{\sigma} = -p\mathbf{I} + 2\eta\mathbf{D}, \tag{5}$$

with p as the pressure, η the dynamic viscosity, and $\mathbf{D}$ the strain rate tensor defined as $\mathbf{D} = (\nabla \boldsymbol{u} + \nabla \boldsymbol{u}^T)/2$. The
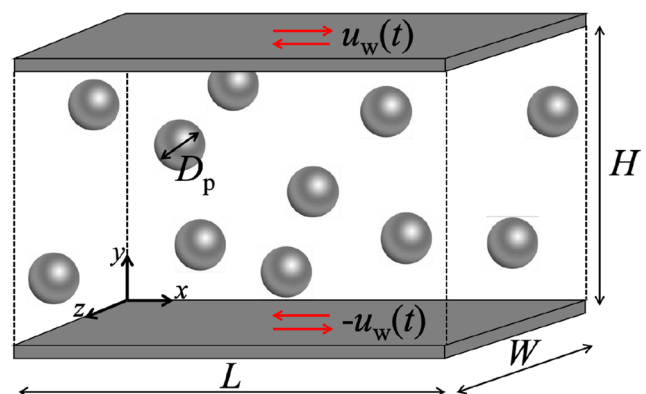

Fig. 1 Schematic picture of a suspension of spherical rigid particles in a Newtonian liquid undergoing oscillatory shear flow

motion of the particles is governed by the Newton-Euler equations. With reference to the generic kth particle, they read

$$\rho_{\mathrm{p}} \mathcal{V}_{\mathrm{p}} \frac{d\mathbf{u}_{\mathrm{p},k}}{dt} = \oint_{\partial P_k} \boldsymbol{\sigma} \cdot \mathbf{n}_k \, dA + \mathbf{F}_k, \tag{6a}$$

$$\mathcal{I}_{\mathrm{p}} \frac{d\boldsymbol{\omega}_{\mathrm{p},k}}{dt} = \oint_{\partial P_k} \mathbf{r}_k \times (\boldsymbol{\sigma} \cdot \mathbf{n}_k) \, dA + \mathbf{T}_k, \tag{6b}$$

where $\mathbf{u}_{\mathrm{p},k}$ is the particle centroid velocity, $\boldsymbol{\omega}_{\mathrm{p},k}$ the particle angular velocity, ∂P_k denotes the particle boundary, dA is a differential surface area element, and ρ_{p}, $\mathcal{I}_{\mathrm{p}}$, and $\mathcal{V}_{\mathrm{p}}$ are the particle density, moment of inertia, and volume, respectively. In particular, for rigid spheres with radius r_{p}, $\mathcal{V}_{\mathrm{p}} = (4/3)\,\pi r_{\mathrm{p}}^3$ and $\mathcal{I}_{\mathrm{p}} = (2/5)\,\rho_{\mathrm{p}} \mathcal{V}_{\mathrm{p}} r_{\mathrm{p}}^2$. In addition, $\mathbf{r}_k$ is the position vector relative to the particle centroid, $\mathbf{n}_k$ is the unit normal vector pointing outwards from the particle, and $\mathbf{F}_k$ and $\mathbf{T}_k$ are the force and torque acting on the particle due to particle-particle and particle-wall interactions. We point out that the density ratio of the suspension ρ_{p}/ρ is considered equal to 1 except where otherwise specified.

The Navier-Stokes and Newton-Euler equations reported above are supplied by the prescribed velocities on the channel sliding walls, at $y = 0$ and $y = H$, and by periodic boundary conditions coupling the channel faces at $x = 0$ and $x = L$ and those at $z = 0$ and $z = W$. The no-slip/no-penetration conditions are imposed on the particle boundaries by the immersed boundary method, as mentioned below. At the initial time, the fluid is considered still and laden with randomly distributed still particles.

The Stokes number can be defined as St $= \rho r_{\mathrm{p}}^2 \omega / \eta$. According to Bird et al. (1987), in a pure Newtonian liquid, inertial effects are negligible when $\mathrm{St}^{1/2}$ is small compared with unity.

Numerical method

The time integration of Eqs. 3–6a is based on an explicit fractional-step method (Kim and Moin 1985), where all the terms are advanced with the third order Runge-Kutta scheme. The governing differential equations are solved on a staggered grid using a second order central finite difference (FD) scheme.

In order to couple the motion of the fluid and the particles, we employ the immersed boundary method (IBM) proposed by Breugem (2012) and used in several previous studies on rigid particle suspensions (see, for example, Picano et al. 2013; Alghalibi et al. 2018). The present IBM is based on the direct-forcing approach,

in which the predicted velocity is corrected using an additional term so as to enforce that the fluid velocity on the surface of the particles matches the velocity of the particles.

In particular, the fluid-solid interaction force reads for the generic kth particle

$$\mathbf{F}_{\mathrm{p},k} = \frac{\mathbf{U}_{\mathrm{p},k} - \mathbf{U}_k}{\Delta t}, \tag{7}$$

where the capital letter is used to indicate that the quantities are computed on the particle surface, i.e. on the nodes of a Lagrangian mesh used to define the particle surface. In the previous relation, $\mathbf{U}_k$ is the interpolated fluid velocity on the Lagrangian points on the particle surface, $\mathbf{U}_{\mathrm{p},k}$ the desired particle velocity in the Lagrangian points ($\mathbf{U}_{\mathrm{p},k} = \mathbf{u}_{\mathrm{p},k} + \boldsymbol{\omega}_{\mathrm{p},k} \times \mathbf{r}_k$), and Δt the time step. The interpolation and spreading between the two grids are performed using the three-dimensional regularized delta function centered on the Lagrangian points first proposed by Roma et al. (1999).

When the distance between two particles is smaller than one Eulerian grid cell, the lubrication force is under-predicted by the IBM due to the finite grid size. To compensate for this inaccuracy and to avoid computationally expensive grid refinements, a lubrication correction model based on the asymptotic analytical expression for the normal lubrication force between spheres is used Jeffrey (1982). A soft-sphere collision model with Coulomb friction takes over the interaction when the particles touch. The restitution coefficients used for normal and tangential collisions are 0.97 and 0.1, respectively, with the Coulomb friction coefficient set to 0.15. More details about these models can be found in the paper by Costa et al. (2015).

A complete description of the numerical scheme and a validation campaign are reported in Izbassarov et al. (2018). In this paper, mesh convergence is achieved with elements of size of $3.125 \times 10^{-2} r_{\mathrm{p}}$, whereas the surface of each particle is resolved through 872 Lagrangian points.

Results

Small amplitude oscillatory shear flow

The xy component of the stress in a suspension undergoing oscillatory shear flow with amplitude γ_0 and frequency ω can be expressed as follows (Macosko and Larson, 1994):

$$\sigma_{\mathrm{xy}}(t) = \gamma_0 \sum_{k=1}^{+\infty} (G'_k \cos(k\omega t) + G''_k \sin(k\omega t)). \tag{8}$$

In the SAOS regime, i.e.,when γ_0 is small, the coefficients $G'_k, G''_k, k = 2, ..., +\infty$, are negligible with respect to G'_1, G''_1; thus, the signal is periodic with one harmonic and the stress can be written as

$$\sigma_{\mathrm{xy}}(t) = \gamma_0 (G' \cos(\omega t) + G'' \sin(\omega t)), \tag{9}$$

with G' as the storage modulus and G'' the loss modulus of the suspension. It is worth remarking that such a definition of the moduli is valid only in the SAOS regime, whereas different definitions apply in the LAOS regime (see below). The condition of SAOS flow implies a linear relationship between the applied strain and the stress response. In other words, in the SAOS regime,

$$\frac{\sigma_{xy}(t)|_{2\gamma_0}}{2\gamma_0} = \frac{\sigma_{xy}(t)|_{\gamma_0}}{\gamma_0}, \qquad (10)$$

which, in turn, implies $(G', G'')|_{2\gamma_0} = (G', G'')|_{\gamma_0}$. We have verified that this condition is fulfilled for $\gamma_0 = 0.005$; thus, the results in this Section are obtained with this value of γ_0.

In Fig. 2, we display the spatial distribution of the particles at $t\omega = 1.0$ in a suspension with $\phi = 0.15$ oscillating at $\gamma_0 = 0.005$ and $St^{1/2} = 0.5$. In panel a, we also display contours of the fluid dimensionless x-velocity $u_x/(H\gamma_0\omega)$ on the channel moving walls, the xy-plane at

(a)

$u_x/(H\gamma_0\omega)$

0.5
0.4
0.3
0.2
0.1
0
-0.1
-0.2
-0.3
-0.4
-0.5

(b)

$u_y/(H\gamma_0\omega)$

0.0035
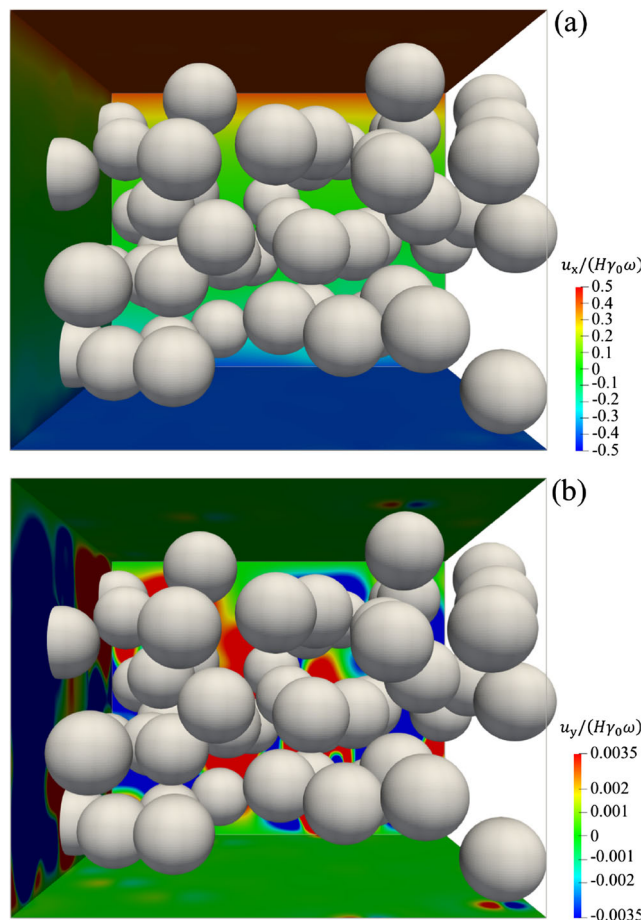0.002
0.001
0
-0.001
-0.002
-0.0035

Fig. 2 Particle distribution at $t\omega = 1.0$ for a suspension with $\phi = 0.15$ oscillating at $\gamma_0 = 0.005$ and $St^{1/2} = 0.5$. **a** Maps of the dimensionless x-component of the fluid velocity on the moving walls, the xy-plane at $z = 0$, and the yz-plane at $x = 0$. **b** Maps of the dimensionless y-component of the fluid velocity on the moving walls, the xy-plane at $z = 0$, and the yz-plane at $x = 0$

$z = 0$, and the yz-plane at $x = 0$, showing that the linear velocity profile that would appear in an inertialess pure Newtonian liquid is here perturbed both due to appreciable inertia (note that $St^{1/2} = 0.5$), which retards the adaptation of the velocity profile in the bulk of the channel to the velocity oscillations imposed at the channel walls, and to the presence of the particles. Panel b of the same figure depicts maps of the fluid dimensionless y-velocity $u_y/(H\gamma_0\omega)$ on the same planes as above, to highlight the fluid velocity perturbations caused by the presence of the particles.

In Fig. 3, we report the temporal history of the shear stress in a suspension oscillating at $\gamma_0 = 0.005$ and $St^{1/2} = 0.5$ for four values of the particle volume fraction from the dilute to the concentrated regime, namely, $\phi = 0.01, 0.05, 0.15, 0.25$. On the horizontal axis, the time is made dimensionless with the oscillatory frequency ω, whereas, on the vertical axis, σ_{xy} is normalized by the loss modulus of the pure suspending liquid $\eta\omega$.

For every ϕ considered, the shear stress undergoes a brief transient, before reaching a periodic regime. In addition, it can be observed that the maximum (respectively, the minimum) stress level increases (respectively decreases) with increasing ϕ and that the stresses corresponding to the different volume fractions are not synchronous; indeed, the greater ϕ, the more the stress curve 'lags' with respect to the applied deformation.

The vertical grey dashed line marks a dimensionless time equal to 4π, i.e. the time needed to the moving walls to perform two oscillatory cycles. Such a time is shown here to be sufficient for the system to reach the periodic regime; for the analysis, we therefore perform regression of the stress data using Eq. 8 starting from the stress value at $t\omega = 4\pi$.

The results of this regression procedure, yielding the moduli introduced above and applied to the different $\sigma_{xy}(t)$ time-traces obtained from the simulations at varying St, are reported in Fig. 4. In panel a, the dimensionless storage
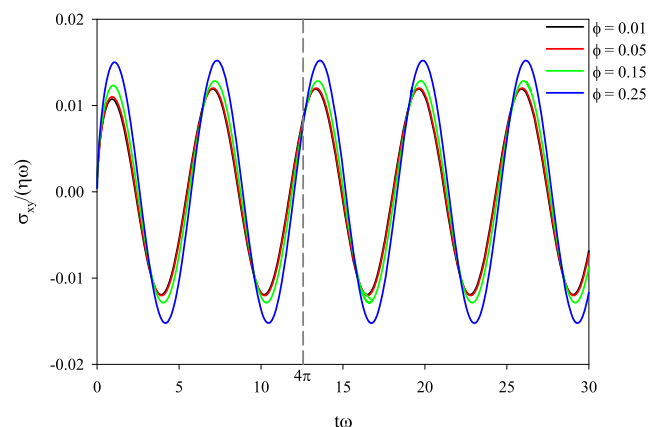

Fig. 3 Shear stress in a suspension oscillating at $\gamma_0 = 0.005$ and $St^{1/2} = 0.5$ for 4 different values of the volume fraction ϕ as indicated in the legend
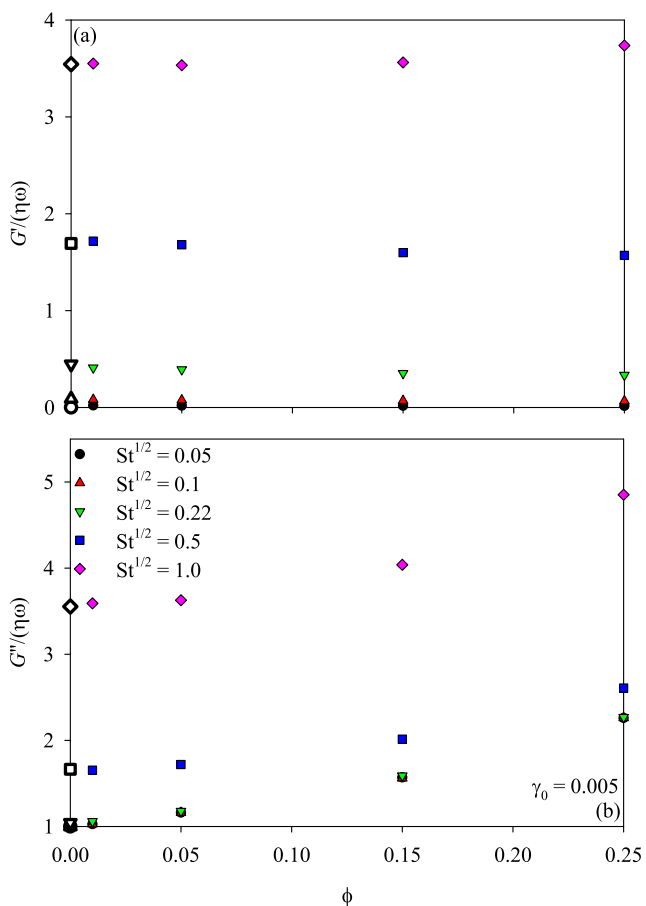
Fig. 4 **a** Dimensionless storage modulus $G'/(\eta\omega)$ and **b** loss modulus $G''/(\eta\omega)$ as a function of the particle volume fraction ϕ for a suspension subjected to SAOS flow at $\gamma_0 = 0.005$. The data pertain the different values of $St^{1/2}$ indicated in the legend. The empty symbols represent the theoretical values for a single-phase fluid given by Böhme and Stenger (1990)

presence of inertia, one can obtain analytically the flow inside the Couette cell and the storage modulus is

$$G' = \mathcal{R}e\left\{\frac{\eta\omega\sqrt{-i\rho\omega H^2/\eta}}{\sinh(\sqrt{i\rho\omega H^2/\eta})}\right\}, \qquad (11)$$

with i the imaginary unit.

The fact that when inertia is non-negligible, the oscillatory measurement 'reads' a non-null value of the storage modulus even in Newtonian fluids/suspensions can be interpreted in terms of inertia acting as an apparent elasticity. Indeed, an analogy can be drawn between inertia and elasticity, because both quantities are related to the idea of 'memory'. In oscillatory flows of viscoelastic fluids, the Deborah number can be defined as the ratio of the liquid relaxation time λ and the flow characteristic time ω^{-1}, i.e. De $= \lambda\omega$. In the limit of vanishing De, fluid relaxation is immediate as compared with the process characteristic time, so no elastic effects can be observed; on the other hand, at non-vanishing De-values, the fluids preserve a 'memory' of its stress state; thus, it is elastic. In the case of a Newtonian fluid in the presence of inertia, the Stokes number is the ratio between the time scale of momentum diffusion $\rho r_p^2/\eta$ and
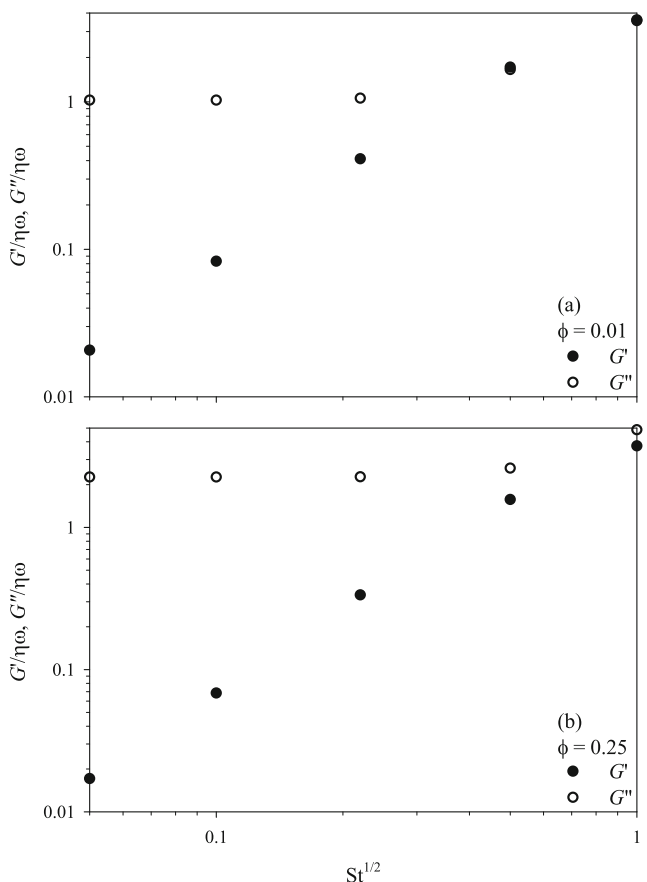
modulus of the suspension, $G'/(\eta\omega)$, is displayed as a function of the particle volume fraction ϕ for the different values of the square root of the Stokes number, $St^{1/2}$, under investigation. As mentioned above, this dimensionless number quantifies the role of inertia. The data in the figure show that for a suspension of rigid particles in a Newtonian liquid, a non-zero storage modulus is always detected when St is not zero. In particular, G' significantly increases with St, whereas it is substantially independent of the particle concentration. In other words, the value of St dictates the level of the modulus G', which is almost constant with ϕ once St is fixed. This suggests that corrections for inertia may be more easily obtained from measurements at a single volume fraction. It is also noteworthy that the plateau values of G' are almost coincident with the theoretical prediction for a single-phase fluid reported by Böhme and Stenger (1990), which is represented on the vertical axis by empty symbols. We point out that, for a single-phase fluid in the

Fig. 5 **a** Dimensionless storage modulus $G'/(\eta\omega)$ and loss modulus $G''/(\eta\omega)$ as a function of $St^{1/2}$ for a suspension subjected to SAOS flow at $\gamma_0 = 0.005$. **a** $\phi = 0.01$, **b** $\phi = 0.25$

the flow characteristic time ω^{-1}. In the limit of vanishing inertia, St $\rightarrow$ 0, momentum diffusion is immediate with respect to the process characteristic time; thus, only a non-null loss modulus can detected, whereas, if the diffusion time is comparable with the oscillatory characteristic time, velocity oscillations in the bulk of the fluid are not in phase with the wall motion and the fluid has 'memory' of the deformation history. On the other hand, there are also some differences between momentum transport in the inertial and the elastic case, which result, e.g. in different effects of normal stresses on the pressure fields (compare, for example, the works from Kulkarni and Morris (2008) and Snijkers et al. (2011)).

In Fig. 5, the dimensionless storage and loss moduli are plotted against St$^{1/2}$ for $\phi = 0.01$ (a) and $\phi = 0.25$ (b), showing that at low particle concentration there is an inertial frequency where G' overlaps with G'' at $O(\text{St}) = 1$, even if there is not a true cross-over as it would occur in viscoelastic liquids at $O(\text{Wi}) = 1$; on the other hand, this is not observed
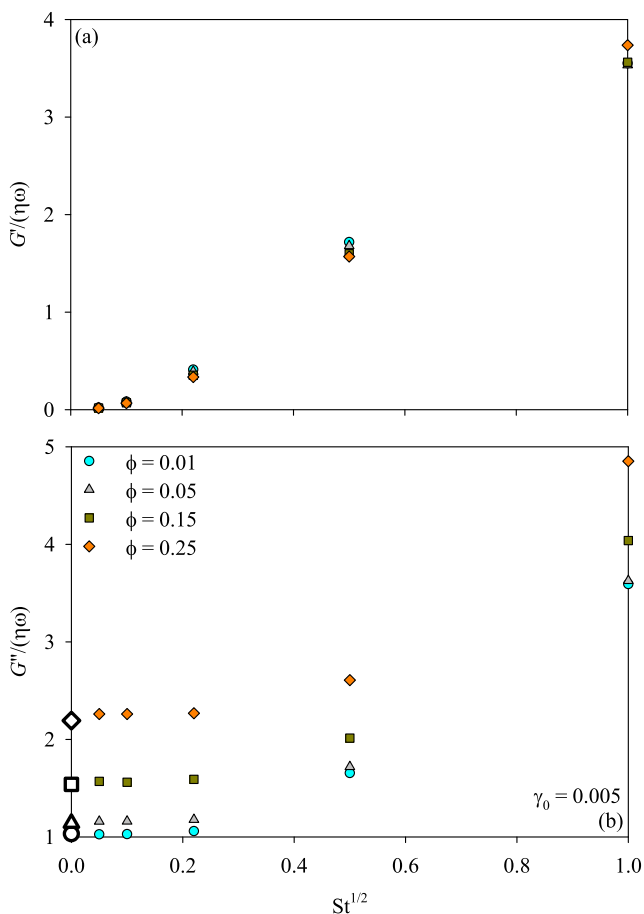

Fig. 7 Temporal evolution of the normalized vertical position of the particles in a suspension with $\phi = 0.15$ oscillating at $\gamma_0 = 0.005$ and St$^{1/2} = 0.5$

Fig. 6 **a** Dimensionless storage modulus $G'/(\eta\omega)$ and **b** loss modulus $G''/(\eta\omega)$ as a function of St$^{1/2}$ for a suspension subjected to SAOS flow at $\gamma_0 = 0.005$. The data pertain the different values of the volume fraction ϕ indicated in the legend. The empty symbols represent the results of the numerical simulations performed by Schaink et al. (2000) and D'Avino et al. (2013) in the inertialess case
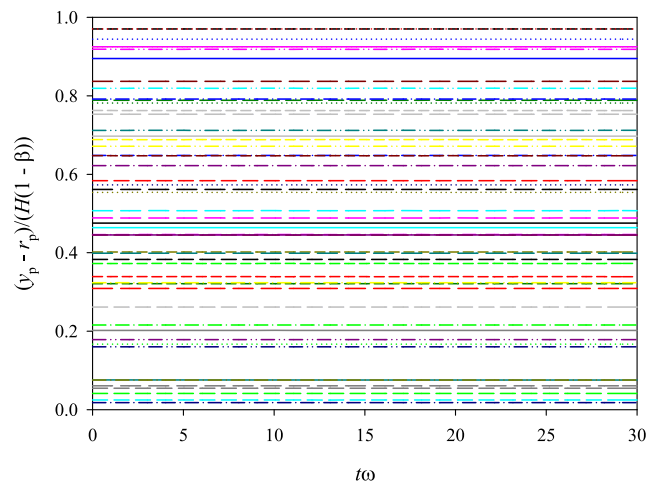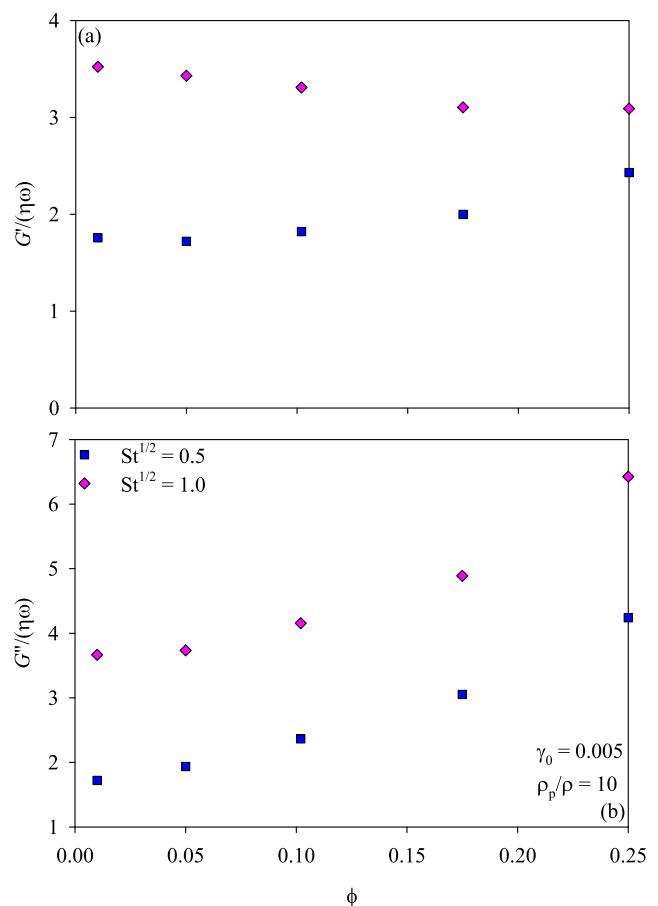

Fig. 8 **a** Dimensionless storage modulus $G'/(\eta\omega)$ and **b** loss modulus $G''/(\eta\omega)$ as a function of the particle volume fraction ϕ for a suspension with $\rho_p/\rho = 10$ subjected to SAOS flow at $\gamma_0 = 0.005$ and St$^{1/2} = 0.5, 1.0$

at high particle volume fraction, where G'' always stays above G' due to extra dissipation from the particles. The dimensionless loss modulus of the suspension, $G''/(\eta\omega)$, is displayed in Fig. 4b: this is quantitatively influenced by both ϕ and St, being an increasing function of both. Moreover, for any fixed St$^{1/2}$, the numerical value of G'' clearly approaches the theoretical value

$$G'' = \mathcal{I}m \left\{ \frac{\eta\omega\sqrt{-i\rho\omega H^2/\eta}}{\sinh(\sqrt{i\rho\omega H^2/\eta})} \right\}, \tag{12}$$

when the particle volume fraction tends to zero (see the empty symbols in Fig. 4b).

The values of the linear viscoelastic moduli shown in Fig. 4 are rearranged and plotted in Fig. 6 as a function of St$^{1/2}$ for the different values of ϕ under consideration. Panel a confirms that G' only depends on St, as the data

at different ϕ collapse on each other. The data in panel b also provide an additional validation of our numerical simulations: indeed, for all the concentration regimes, when St$^{1/2}$ tends to zero, the values of G'' tend to the numerical values computed in the inertialess case by Schaink et al. (2000) by means of Stokesian dynamics and by D'Avino et al. (2013) with a finite element implementation of the Stokes equations. The data in Fig. 6b also show that, for every particle volume fraction, G'' is almost constant for St$^{1/2}$ below about 0.2, which identifies, then, the threshold above which inertial effects actually affect the loss modulus of the suspension.

In the literature, it is well known that, in the presence of inertia, cross-streamline migration occurs to rigid particles in sheared Newtonian fluids (see, for example, McLaughlin 1993). As a consequence, inertia is expected to alter the particle random distribution in the flow cell, since all the


Fig. 9 **a** Shear stress in a suspension at $\phi = 0.25$ and St$^{1/2} = 0.5$ for $\gamma_0 = 0.005, 0.1, 1.0$. **b** Lissajous curves at $\phi = 0.25$ and St$^{1/2} = 0.5$ for $\gamma_0 = 0.005, 1.0$
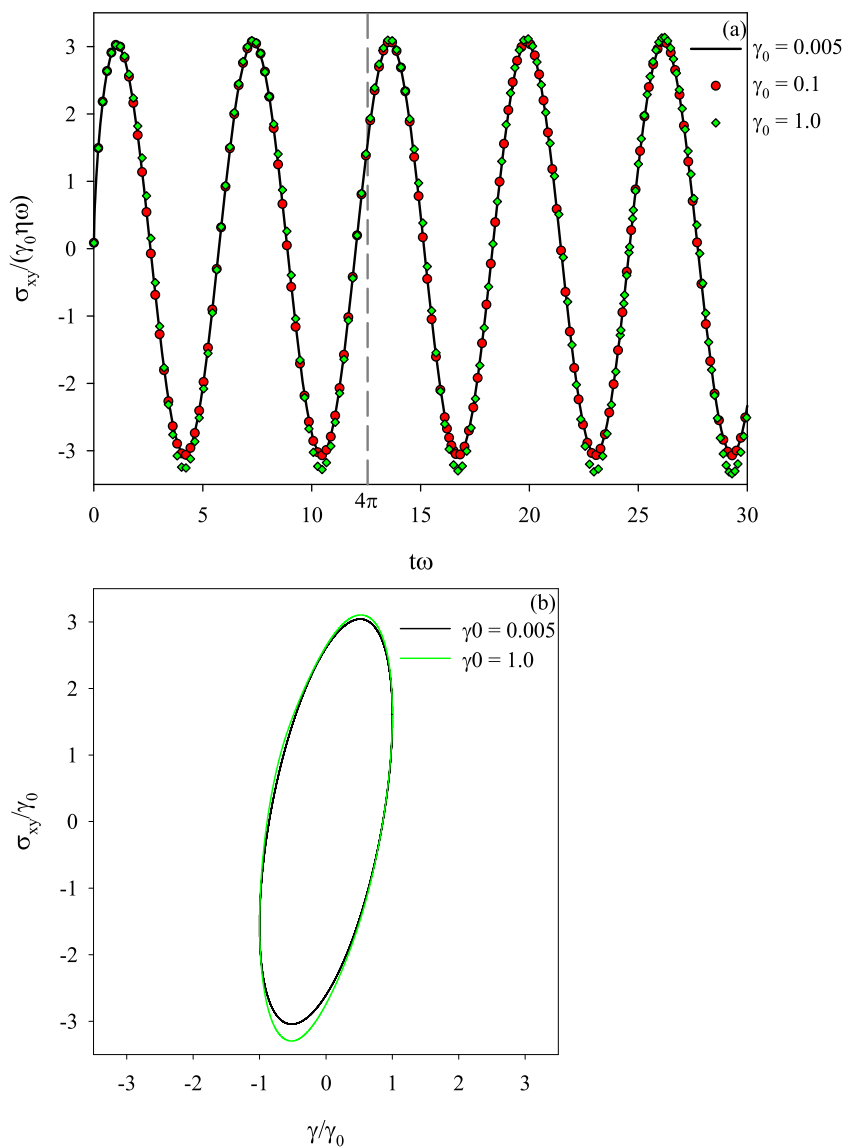
particles would be deterministically pushed towards two equilibrium heights along the channel gap, thus influencing the shear stress in the suspension. However, due to the very little amplitude of the oscillations, lateral migration does not

play any role for the oscillatory shear flow considered here. As an illustrative example, we show in Fig. 7 the temporal evolution of the vertical positions of all the particles in the flow cell normalized over the available space along the

Fig. 10 Temporal evolution of the normalized vertical positions of the particles in a suspension with $\phi = 0.25$ oscillating at $St^{1/2} = 0.5$ and $\gamma_0 = 0.005$ (**a**), 0.1 (**b**), 1.0 (**c**).
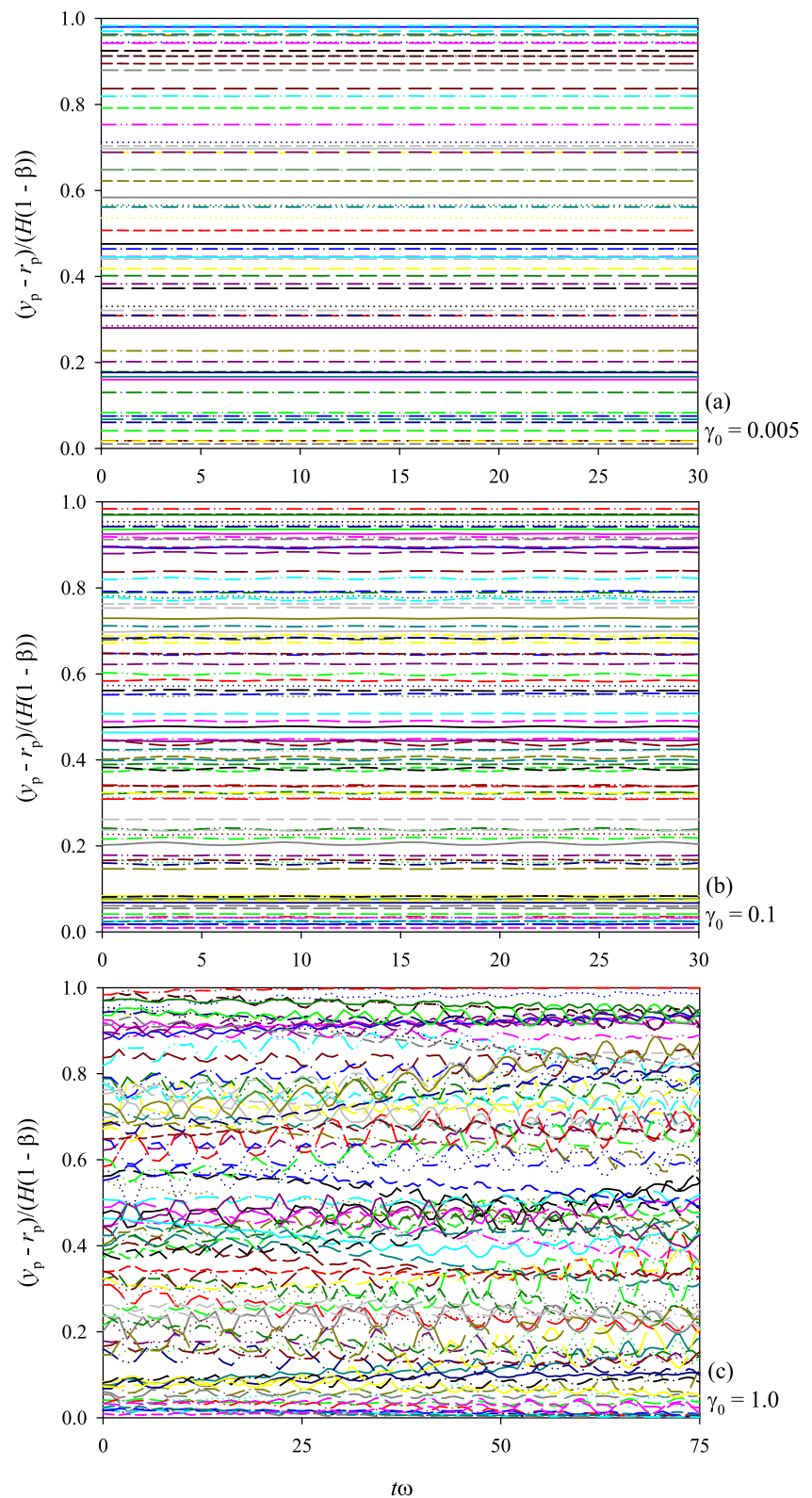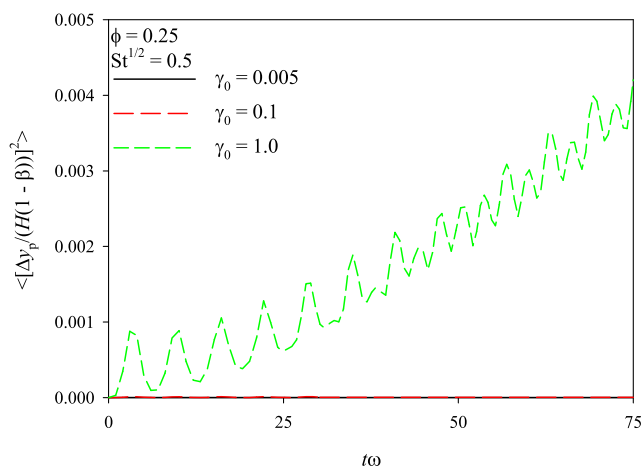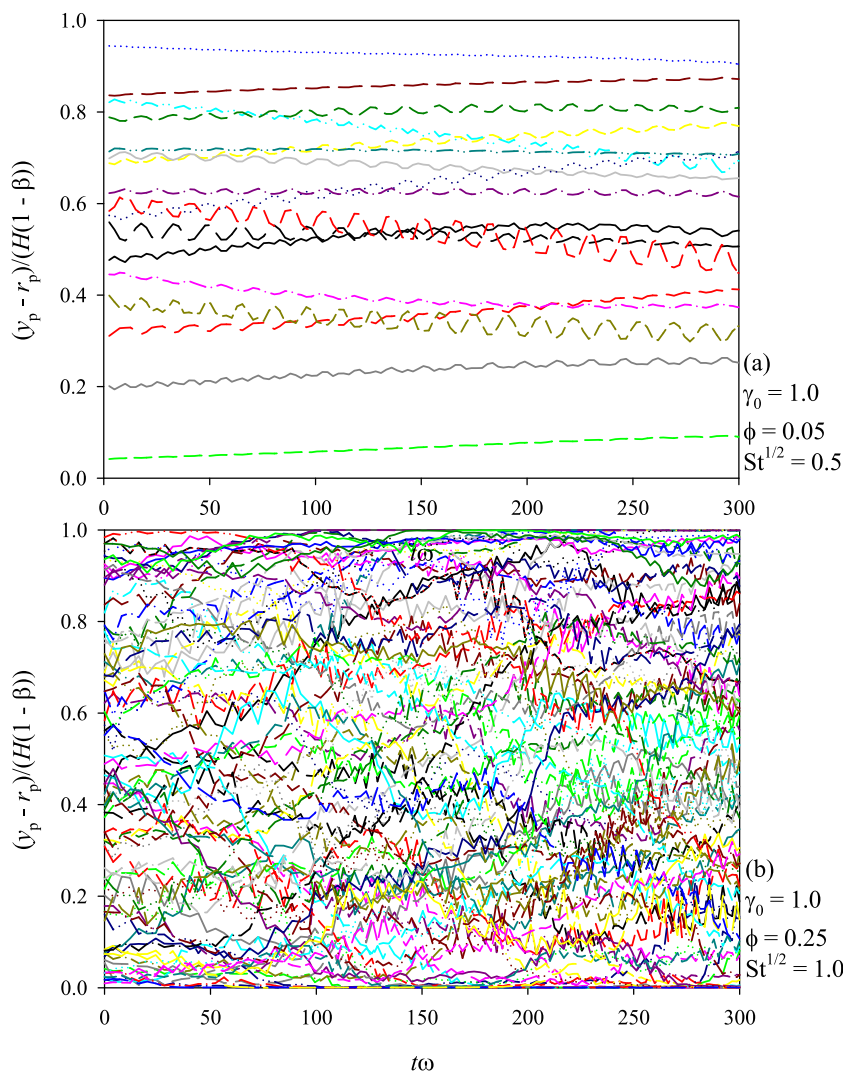
Fig. 11 Temporal evolution of the mean square normalized vertical displacement of the particles in a suspension with $\phi = 0.25$ oscillating at $St^{1/2} = 0.5$ and $\gamma_0 = 0.005, 0.1, 1.0$

channel gap $(y_p - r_p)/(H(1 - \beta))$ in a suspension with $\phi = 0.15$ oscillating at $\gamma_0 = 0.005$ and $St^{1/2} = 0.5$. No displacement in the wall-normal direction can be detected for any of the particles in the flow cell.

In the cases shown and discussed above, G' does not depend on ϕ: this is probably due to the fact that, for suspensions of neutrally buoyant particles, inertia acting on the scale of the suspension volume has always the same effect on the apparent elastic modulus of the system. In Fig. 8, we plot G' and G'' as a function of ϕ at $St^{1/2} = 0.5$ and 1.0 for a suspension of particles ten times denser than the suspending liquid. In Fig. 8a, it is apparent that in the dilute regime, the storage modulus is slightly larger than in the case of a density-matched suspension (see Fig. 4a), then, when ϕ increases, there is a non-trivial concentration-dependent effect due to additional inertial contributions on the scale of the particles. Indeed, at $St^{1/2} = 0.5$, G' increases with ϕ, whereas it decreases with ϕ at $St^{1/2} = 1.0$.

Fig. 12 Temporal evolution of the normalized vertical positions of the particles in a suspension with $\phi = 0.05$ oscillating at $St^{1/2} = 0.5$ and $\gamma_0 = 1.0$ (**a**) and a suspension with $\phi = 0.25$ oscillating at $St^{1/2} = 1.0$ and $\gamma_0 = 1.0$ (**b**)

On the other hand, it can be seen from Fig. 8b that at $\rho_p/\rho = 10$, G'' has an analogous behaviour than at $\rho_p/\rho = 1$ for both $St^{1/2} = 0.5$ and 1.0, though with larger values.

Large amplitude oscillatory shear flow

In this section, we extend our study to suspensions subjected to LAOS flow.

Figure 9 a reports the dimensionless shear stress $\sigma_{xy}/(\eta\omega)$ normalised by the oscillatory amplitude γ_0 as a function of the dimensionless time $t\omega$ in a suspension with $\phi = 0.25$ oscillating at $St^{1/2} = 0.5$. Values of γ_0 varying by three orders of magnitude are considered, i.e. $\gamma_0 = 0.005$ (SAOS regime), 0.1, and 1.0. It can be inferred from the

data in Fig. 9 that at $\gamma_0 = 0.1$, the system is still in the SAOS regime, because the red circles pertaining this amplitude collapse on the black curve pertaining the stress for $\gamma_0 = 0.005$ (see Eq. 10). The condition on linear stress in Eq. 10, on the other hand, does not hold for the stress time traces at $\gamma_0 = 1.0$ (green diamonds); thus, the system is in the LAOS regime for this value of the oscillatory amplitude. As a further proof, we display in Fig. 9b the Lissajous curve for $\gamma_0 = 0.005$, which appears elliptical, and $\gamma_0 = 1.0$, which is no longer elliptical and does not superimpose to the one at $\gamma_0 = 0.005$, even if the discrepancy is not very large.

Such loss of linearity can be investigated by looking at the temporal evolution of the particle vertical positions displayed in Fig. 10. As discussed above, no lateral
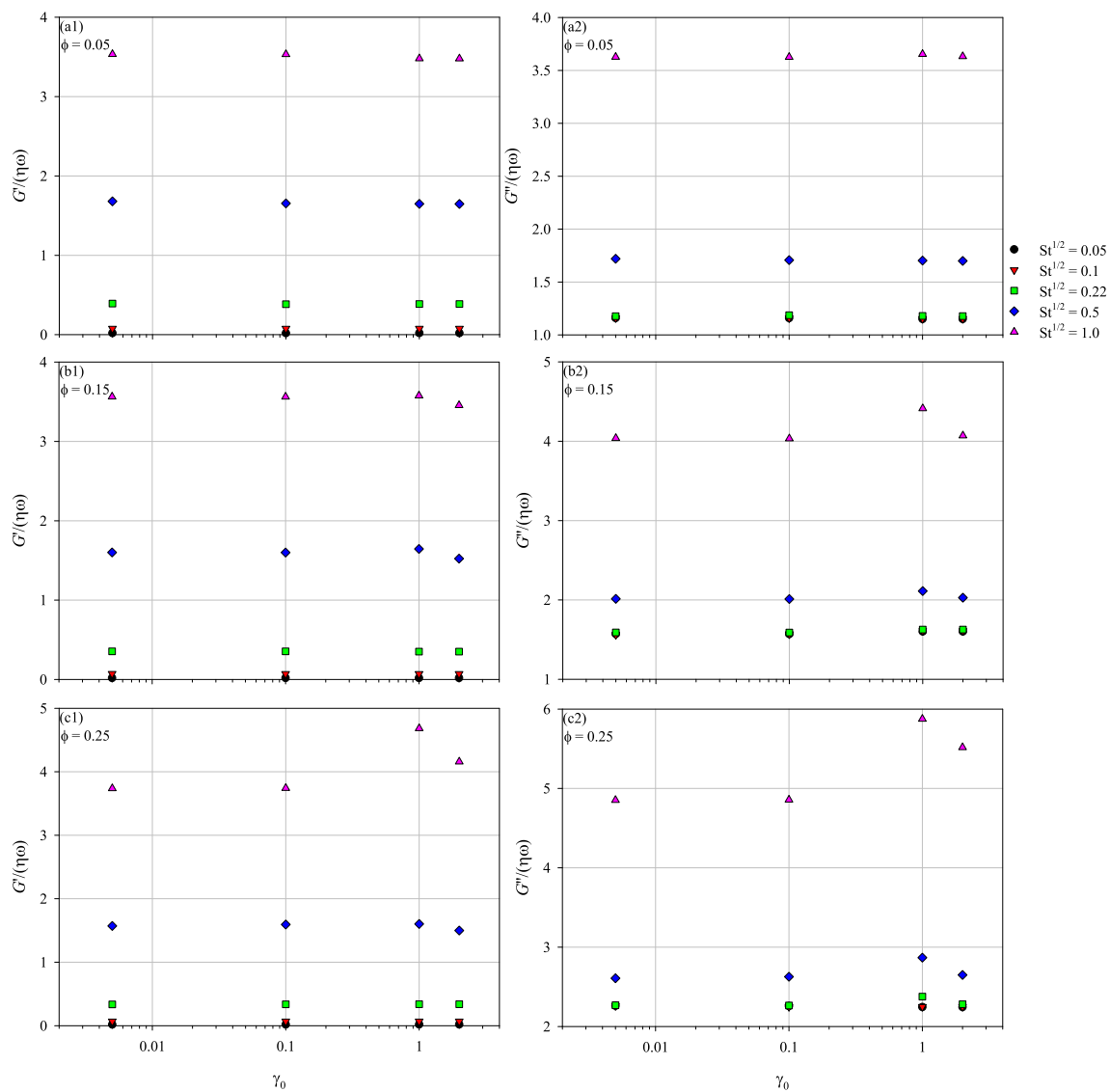

Fig. 13 Dimensionless storage modulus $G'/(\eta\omega)$ (left column) and loss modulus $G''/(\eta\omega)$ (right column) as a function of the oscillatory amplitude γ_0. **a** Top row: Dilute suspension at $\phi = 0.05$, **b** middle row: semi-dilute suspension at $\phi = 0.15$, **c** bottom row: concentrated suspension at $\phi = 0.25$. In each panel, the data are reported for the different values of $St^{1/2}$ under investigation

migration is observed for small deformations, see data for $\gamma_0 = 0.005$ in Fig. 10a. Conversely, for $\gamma_0 = 0.1$, we do not observe any migration only for some of the particles, whereas others exhibit oscillations of their vertical position with the same frequency as the applied shear, yet such oscillations yield no net displacement in the wall-normal direction over our observation time (see Fig. 10b.

However, as deduced from Fig. 10c, the particle vertical positions considerably oscillate and display a net displacement over several periods for $\gamma_0 = 1.0$. Moreover, both the oscillations and the net wall-normal displacement appear irregular, which could be ascribed to the complex hydrodynamic interactions mediated by fluid inertia arising among the particles while they travel back and forth along the streamwise direction. Hence, the microstructure of the system changes in time.

A quantitative measure of the irreversible net displacement of the particles in the wall-normal direction is given in Fig. 11, where the temporal evolution of the mean square normalized vertical displacement of the particles is plotted parametric in the oscillatory amplitude. Such quantity is obtained by computing at each time value the average of the square vertical displacements of all the particles appearing in the computational domain with respect to their initial vertical positions. It is apparent that at $\gamma_0 = 0.005$ and 0.1, the mean square displacement of the particles is null, namely, the beads keep their vertical positions along the cycles, whereas in the non-linear regime, i.e. at $\gamma_0 = 1.0$, it has an irregular oscillatory behaviour (see above) with its value increasing in time, which indicates an irreversible displacement of the particles from their initial vertical positions. Something analogous had been observed by Pine et al. (2005) for suspensions of rigid particles under steady shear flow (with no oscillations), yet in that case, since inertia is negligible, the irreversible displacement of the particles only occurs above a certain threshold in concentration due to multiple particle interactions that break the symmetry of the system.

In order to further elucidate the effects of solid volume fraction and fluid inertia on the aforementioned oscillations, we report in Fig. 12 the temporal evolution of the vertical positions of the particles at $\gamma_0 = 1.0$ for $\phi = 0.05$, $St^{1/2} = 0.5$ (a) and $\phi = 0.25$, $St^{1/2} = 1.0$ (b). By comparing Fig. 12a–b with Fig. 10c, it is apparent that decreasing the solid volume fraction from 0.25 to 0.05 at $\gamma_0 = 1.0$ and $St^{1/2} = 0.5$ has no particular qualitative effect on the particle oscillations, whereas increasing $St^{1/2}$ from 0.5 to 1.0 at $\gamma_0 = 1.0$ and $\phi = 0.25$ significantly enhances the irregularity of particle oscillations and their net displacement in the wall-normal direction; thus, inertia has a much more relevant effect on the time evolution of the microstructure of the suspension.

We perform a regression of the stress data in Fig. 9 starting from $t\omega = 4\pi$. However, it should be noted

that, while in the SAOS regime the definition of (and the procedure to compute) the moduli G' and G'' is univocal (see Eq. 9), this is not the case in the LAOS regime. Indeed, the way of determining G' and G'' in LAOS is still debated (see, for example, the review by Hyun et al. 2011, and references therein). In this work, we adopt the procedure proposed by D'Avino et al. (2013), namely, we calculate the moduli of the suspension by fitting the oscillatory stress curves through the single-harmonic wave given by Eq. 9 also in the LAOS regime.

In Fig. 13, we display the values of the dimensionless storage modulus $G'/(\eta\omega)$ (left column) and loss modulus $G''/(\eta\omega)$ (right column) as a function of the oscillatory amplitude γ_0 for three values of the particle volume fraction ϕ, namely, $\phi = 0.05$ (top row), 0.15 (middle row), and 0.25 (bottom row), for different values of $St^{1/2}$.

First, we note that large amplitude effects are negligible for the dilute suspension at $\phi = 0.05$, i.e. the moduli are almost independent of γ_0 for every value of $St^{1/2}$. For the medium-concentration suspension at $\phi = 0.15$, some
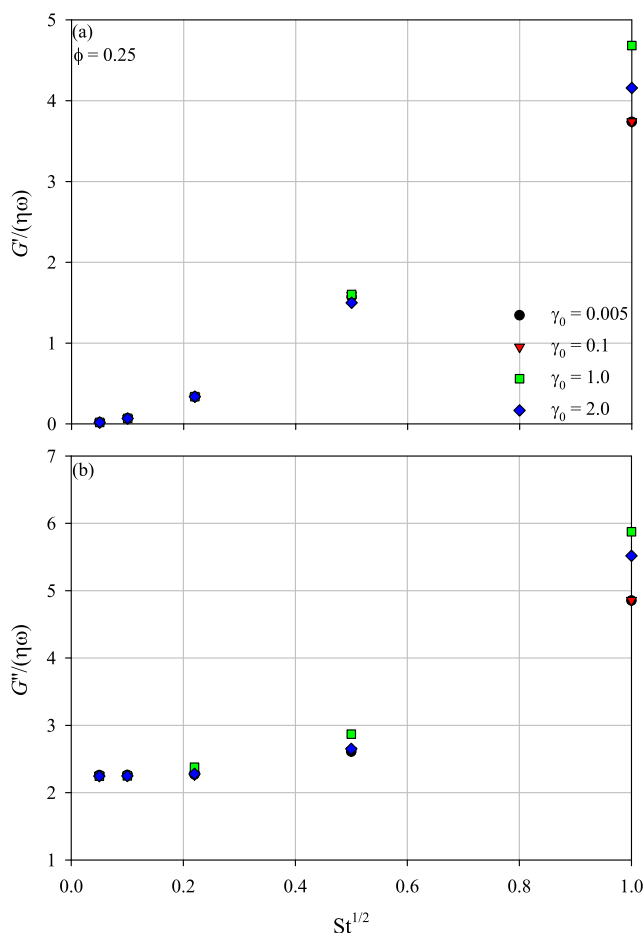

Fig. 14 Dimensionless storage modulus $G'/(\eta\omega)$ (**a**) and loss modulus $G''/(\eta\omega)$ (**b**) as a function of $St^{1/2}$ for a concentrated suspension at $\phi = 0.25$ parametric in the oscillatory amplitude γ_0

effects of γ_0 can be seen at $St^{1/2} = 0.5$ and 1.0, i.e. the cases where inertia is more relevant; in particular, both the moduli have an overshoot at $\gamma_0 = 1.0$, then decrease as the deformation amplitude is further increased. Such effect is mostly visible on G'' at $St^{1/2} = 1.0$. Again, an analogy can be found with viscoelastic systems, since a non-monotonic behaviour of $G''(\gamma_0)$ has been reported by D'Avino et al. (2013) for LAOS flow of suspensions of rigid spheres in a viscoelastic liquid. When the solid concentration is equal to 0.25, this behaviour of the moduli is enhanced and it can be (moderately) seen even at lower inertia, i.e. already at $St^{1/2} = 0.22$. In summary, since the non-linear effects detected in LAOS flow are related to the hydrodynamic interactions among particles mediated by fluid inertia, those effects are enhanced when hydrodynamic interactions are enhanced, thus at increasing particle concentration (ϕ) and inertia (St). This is also shown in Fig. 14, where the dimensionless values of the storage modulus and the loss modulus are plotted for a concentrated suspension at $\phi = 0.25$ as a function of $St^{1/2}$ parametric in the oscillatory amplitude γ_0.

Conclusions

In this paper, we investigate by means of interface-resolved numerical simulations the effects of inertia, quantified by the Stokes number St, on the measured apparent viscoelastic moduli of suspensions of mono-disperse non-colloidal rigid spherical particles in a Newtonian liquid from the dilute to the concentrated regime. We first consider the SAOS flow and then extend the analysis to LAOS flow.

In the SAOS regime, even if the system is constituted by rigid particles in a Newtonian liquid, we always detect a non-zero storage modulus, i.e. viscous momentum diffusion acts as an apparent elasticity in an inertial flow. An analogy can be made between momentum diffusion time scale and elastic time scale, because both are related to the idea of memory, so that the Stokes number can be interpreted in analogy to the Deborah number defined for oscillatory flow of a viscoelastic liquid; indeed, it relates a relaxation time scale (here, the momentum diffusion time) and a flow time scale. In particular, G' significantly increases with the Stokes number St, whereas it depends on the particle volume fraction only in suspensions of particles denser than the fluid. On the other hand, the loss modulus of the suspension G'' increases with both ϕ and St. When the particle volume fraction tends to zero, our numerical results approach the theoretical values given by Böhme and Stenger (1990), whereas, when St vanishes, they tend to the numerical results computed by Schaink et al. (2000) and D'Avino et al. (2013) in the inertialess case.

The amplitude of the imposed oscillations is then increased to investigate the suspension behavior in LAOS flow. Our data indicate that the moduli are almost independent of the deformation amplitude for a dilute suspension, $\phi=0.05$. For a suspension of medium concentration, $\phi=0.15$, G' and G'' change non-monotonically with the deformation γ_0 at high St, namely, when inertia is more relevant. When the concentration is further increased, such effects are enhanced. In addition, our simulations show that, when the oscillatory amplitude is large, particles display a wall-normal net displacement from their initial position due to hydrodynamic interactions mediated by fluid inertia, which changes the system microstructure.

In summary, our simulations show that suspended particles increase the measured loss modulus in small-amplitude oscillatory shear, while only inertia affects the storage modulus in this regime. In large-amplitude oscillatory shear, however, we show that both storage and loss moduli are increasingly affected when Stokes number and particle concentration increase due to particle-particle interactions.

References

Alghalibi D, Lashgari I, Brandt L, Hormozi S (2018) Interface-resolved simulations of particle suspensions in newtonian, shear thinning and shear thickening carrier fluids. J Fluid Mech 852:329–357

Barnes HA (2003) A review of the rheology of filled viscoelastic systems. Rheology Reviews:1–36

Bird RB, Armstrong RC, Hassager O (1987) Dynamics of polymeric liquids. Vol 1: Fluid mechanics. Wiley, New York

Böhme G, Stenger M (1990) On the influence of fluid inertia in oscillatory rheometry. J Rheol 34(3):415–424

Breugem WP (2012) A second-order accurate immersed boundary method for fully resolved simulations of particle-laden flows. J Comput Phys 231(13):4469–4498

Costa P, Boersma BJ, Westerweel J, Breugem WP (2015) Collision model for fully resolved simulations of flows laden with finite-size particles. Phys Rev E 92(5):053,012

D'Avino G, Greco F, Hulsen MA, Maffettone PL (2013) Rheology of viscoelastic suspensions of spheres under small and large amplitude oscillatory shear by numerical simulations. J Rheol 57(3):813–839

Einstein A (1911) Berichtigung zu meiner arbeit: eine neue bestimmung der moleküldimensionen. Ann Phys 339(3):591–592

Hyun K, Wilhelm M, Klein CO, Cho KS, Nam JG, Ahn KH, Lee SJ, Ewoldt RH, McKinley GH (2011) A review of nonlinear oscillatory shear tests: analysis and application of large amplitude oscillatory shear (laos). Prog Polym Sci 36(12):1697–1753

Izbassarov D, Rosti ME, Ardekani MN, Sarabian M, Hormozi S, Brandt L, Tammisola O (2018) Computational modeling of multiphase viscoelastic and elastoviscoplastic flows. Int J Numer Methods Fluids 88(12):521–543

Jeffrey D (1982) Low-reynolds-number flow between converging spheres. Mathematika 29(1):58–66

Kim J, Moin P (1985) Application of a fractional-step method to incompressible navier-stokes equations. J Comput Phys 59(2):308–323

Kulkarni PM, Morris JF (2008) Suspension properties at finite reynolds number from simulated shear flow. Phys Fluids 20(4):040,602

Macosko CW, Larson RG (1994) Rheology: principles, measurements, and applications, Vch, New York

McLaughlin JB (1993) The lift on a small sphere in wall-bounded linear shear flows. J Fluid Mech 246:249–265

Mewis J, Wagner NJ (2009) Current trends in suspension rheology. J Non-Newton Fluid Mech 157(3):147–150

Picano F, Breugem WP, Mitra D, Brandt L (2013) Shear thickening in non-brownian suspensions: an excluded volume effect. Phys Rev Lett 111(9):098,302

Pine DJ, Gollub JP, Brady JF, Leshansky AM (2005) Chaos and threshold for irreversibility in sheared suspensions. Nature 438(7070):997

Roma AM, Peskin CS, Berger MJ (1999) An adaptive version of the immersed boundary method. J Comput Phys 153(2):509 – 534. https://doi.org/10.1006/jcph.1999.6293, http://www.sciencedirect.com/science/article/pii/S0021999199962939

Rosti ME, Brandt L (2018) Suspensions of deformable particles in a couette flow. J Non-Newton Fluid Mech 262:3–11

Schaink HM, Slot JJM, Jongschaap RJJ, Mellema J (2000) The rheology of systems containing rigid spheres suspended in both viscous and viscoelastic media, studied by stokesian dynamics simulations. J Rheol 44(3):473–498

Snijkers F, D'Avino G, Maffettone P, Greco F, Hulsen M, Vermant J (2011) Effect of viscoelasticity on the rotation of a sphere in shear flow. J Non-Newton Fluid Mech 166(7-8):363–372

Tanner RI (2018) Aspects of non-colloidal suspension rheology. Phys Fluids 30(10):101,301